

Broadband antireflection and self-cleaning random grass structure on silicon

X. YE^{a*}, J. HUANG^a, R.F. NI^{a,b}, Z. YI^{a,b}, X. D. JIANG^a, W. G. ZHENG^a

^aResearch Center of Laser Fusion, China Academy of Engineering Physics, Mianyang 621900, China

^bJoint Laboratory for Extreme Conditions Matter Properties, Southwest University of Science and Technology and Research Center of Laser Fusion, CAEP, Mianyang 621900, China

We have developed a simple and scalable approach for fabricating random antireflective grass structures on silicon substrates. These structures are prepared by a two-step dry etching process. And they exhibit excellent broadband antireflection properties. The results show that the reflection of silicon wafer with the grass structures can be reduced to about 0.5% in the range UV to near-IR wavelength (300–1500 nm). Besides, the antireflective grass surfaces possess superhydrophobic properties. Such antireflective grass surfaces are promising for fabrication of antireflective and self-cleaning optical materials to be used in many important fields.

(Received December 19, 2014; accepted January 21, 2015)

Keywords: Broadband antireflection, Self-cleaning, Random grass, Reactive ion etch, Deep reactive ion etch

1. Introduction

Conventionally, there has been considerable interest in broadband antireflection properties for a variety of device applications such as liquid crystal displays, high-performance solar cells, detecting optoelectronic and surface emitting devices [1]. Recently, there has been a major research to improve the cell efficiency of solar cells around the environment, especially for silicon based solar cells due to the low cost [2]. A polished substrate surface of an optical device can reduce the scattering loss effectively. However, there is still a Fresnel reflection loss at the optical interface between two medium of different refractive index as consequence of sudden change of the refractive index at a discontinuous boundary [3]. Anti-reflection (AR) technology is currently used to reduce reflectance from the surface of solar cells [4]. The current AR technologies can be broadly divided into two categories: one is AR coatings, and another is subwavelength surface texturing [5-9]. However, the AR coatings has problems associated with limitations in the coating materials and various physical and chemical properties that will affect adhesion, thermal mismatch, and the stability of the thin-film stacks [10-12]. On the other hand, the subwavelength surface texturing possesses distinct advantages compared to the AR coatings. First, the subwavelength surface texturing typically consist of various fractions of air and substrate

material [6]. However, in the field of optics or photoelectron, refractive index of optical materials is very high and proper materials for antireflective coatings based on multilayered films are rare in nature [12]. Second, the subwavelength surface texturing exhibits robust mechanical stability and better durability than AR coatings because no foreign materials are involved when they are etched in the substrate [13]. Last, the subwavelength surface texturing have many tunable factors, such as the depth, period and the substrate filling factor [14]. They can dramatically suppress the reflection losses over a large angle of incidence and a large range of wavelength because of with gradually changing refractive indices moving from that of the incident medium to that of the substrate [15]. But the thin film AR coatings based on porous or multilayered films demand thicker and more layers to obtain broadband antireflective properties. Thus, the preparation of such coatings is inefficient and high cost [16]. To obtain the subwavelength surface texturing with a broadband antireflection properties, many fabrication methods have been proposed, including interference lithography [17], electron beam lithography [18, 19], colloidal nanosphere lithography [20], anodic porous alumina [21], thermally dewetting [22] and magnetron sputter deposition [23] metallic nanoparticles as etch masks followed by plasma etching. However, these methods are restricted for requiring complications multiple steps, high cost and low

effective for practical applications. In practical applications, when contamination occurs on AR surfaces, their optical properties would dramatically deteriorate. Contaminants accumulate on the surface leading to scattering and reflection of light. This problem may be solved by creation of a surface that has superhydrophobic property. The AR property and self-cleaning surfaces are highly desired to various optical and photoelectron devices [24]. In the previous study, some researcher reported a new fabrication approaches especially low-cost, maskless, and fabrication methods for antireflective surfaces with a low aspect ratio [25]. However, it is well-known that achieving a deeper tapered shape offers a better suppression of reflection [26].

In this paper, we improve two-step dry etch process to produce high aspect ratio silicon random grass. In the first step, low aspect ratio silicon random grass was produced by reactive ion etch (RIE) process, the second step will be referred to as the deep reactive ion etch (DRIE) for high aspect ratio silicon grass. We will describe the antireflection surface fabrication technique, the optical characteristics and superhydrophobicity for self-cleaning property of the silicon grass surface.

2. Materials and method

The silicon substrates were polished (roughness value below 1nm), and soaked in the mixture of 98% H_2SO_4 / 30% H_2O_2 (volumetric ratio 3:1) for 30 min under boiling (with ultrasonic wave), and then rinsed with deionized water ($18.2 \text{ M}\Omega \text{ cm}^{-1}$) several times and dried with N_2 stream. All chemicals (analytical grade) were supplied by Aldrich and used without further purification. Deionized and doubly distilled water was used throughout the experiments.

Substrates were then etched on the Plasmalab Oxford 100 plus (ICP 180) system (Oxford Instrument Co., UK). In the RIE step, the gases were SF_6 (20 sccm), CHF_3 (10 sccm) and O_2 (15sccm), the coil RF power was 400 W, the Platen RF power was 0 W, and the chamber pressure was 50 mTorr. This process causes the etching of a certain low grass on the substrate in randomly distributed sites. In the next step, the substrate with the randomly low grass is subjected to a deep reactive ion etching process (DRIE), which uses alternate cycles of etching and passivation. The etching step gases were SF_6 (20sccm) and O_2 (15sccm), and the passivation step gases was C_4F_8 (30sccm). The coil RF power was 400W, the Platen RF power was 15W. And the etching/passivation active time was 5/4s.

The chamber pressure was 20mtorr. The grass grown in the RIE step becomes more higher in the DRIE step.

SEM micrographs were taken with a JEOL FESEM6700F electron microscope with primary electron energy of 5 kV. A Shimadzu 3600 UV-vis-NIR spectrophotometer with standard mirror optics was used to measure the specular reflectance in the 300-1500 nm range at the incidence angle of 8° .

Water droplets of 3 μL were used for the contact angle (CA) measurements. All of the measurements were performed at room temperature using a drop shape analysis system. At least five measurements were averaged for all of the data reported here. Before measurement, the samples were cleaned using O_2 plasma for 12 min.

3. Result and discussion

RIE grass occurs when an etch resistant material accumulates in small patches on the sample surface. These patches cause micro-etch-masking, which results in formation of cones. The basic mechanism of cone formation during plasma etching has been understood. Previous reports have identified the cause of RIE grass as sputter re-deposition of chamber materials, cathode materials and polymer formation. Under certain plasma conditions, carbon-fluorine polymers can form on silicon surface. The polymers can micro-etch mask the sample surface and produce RIE grass [27].

In the process of RIE, the polymers act as masks (Fig. 1a), but they can also be etched by the reactive ions. In the beginning, the silicon grasses are formed by etching of reactive ions. During the etching, the size of the polymers decreases, leading to the formation of cone-shaped profiles. And the polymers will form randomly on the surface again, during the RIE process (Fig. 1b). This RIE process causes hardly growth of polymers on the "V"-shape profiles of the grooves. Therefore the RIE grass commonly has the appearance of a low aspect ratio (Fig. 1b).

And in the next step, the substrate with the randomly distributed RIE grass is subjected to a deep reactive ion etching process (DRIE), which uses alternate cycles of etching and passivation. After DRIE process, this causes dramatic-looking, tall silicon spike-like structures with sharp tips, as shown in Fig. 1 C. Because of the DRIE process, these tips exhibit scalloping along their height, which gives them the corkscrew-like appearance.

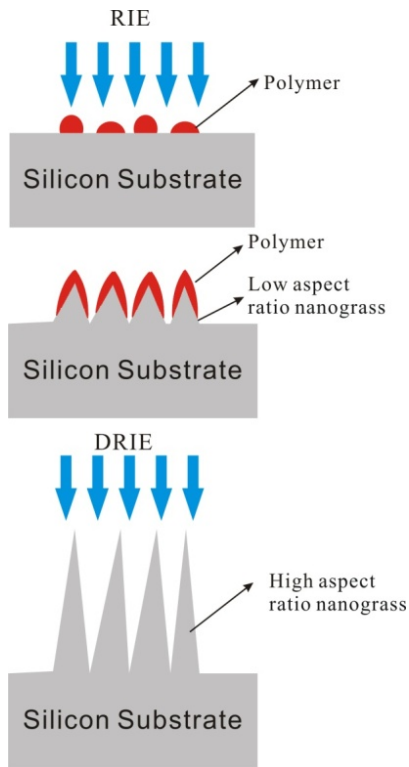


Fig. 1. Schematic illustration of the process for preparing grass structures

Fig. 2 shows the morphology of the grass on silicon substrate. The left side show that silicon grass was successfully fabricated using RIE process. And the right side is SEM of the grass on silicon fabricated by DRIE step. Fig. 2(A B) are top view SEM images of silicon grass. We can see that the silicon grass arrays on the substrate in randomly distributed sites. The silicon grass is characterized by high uniformity and the diameter of the grass was about from submicron to micron. The cross-sectional SEM image in Fig. 2(C) shows that the average height of silicon grass on silicon produced by RIE is about 600nm. These silicon grasses look like short, low aspect ratio (about 1.0) and the tapered profile. After 8 min of DRIE process time, this causes dramatic-looking, tall silicon spike like structures with sharp tips of about 50 nm diameter, as shown in Fig. 2(D). Because of the DRIE process, these tips exhibit scalloping along their height, which gives them the corkscrew-like appearance. Depending on the duration of DRIE, these grasses can be fabricated to heights in excess of 5 μm . The grasses on silicon with aspect ration as high as ~ 5.0 can be easily fabricated by the Bosch DRIE approach. In Fig. 2(E F), the SEM image of the angled view of the tapered grasses array fabricated in the large area is shown. Considering the

fabrication process is composed of two step etching without costly and time-consuming patterning steps such as electron beam lithography or nanoimprint lithography, the tapered grass fabrication could be easily extended to wafer scale larger area.

In an $\text{SF}_6/\text{O}_2/\text{CHF}_3$ plasma of RIE process, there is a constant competition between the fluorine radicals that etch and the oxygen radicals that passivate the silicon[28]. At a certain oxygen content there is such a balance between the etching and the passivation that a grass on substrate surface (Fig. 2 left side) . At the same moment native sputtering, polymer, etc. will act as micromasks and grass will appear because of the directional etching. These grasses consist of a silicon body with a thin passivating silicon oxyfluoride skin , as shown in Fig.1 B.

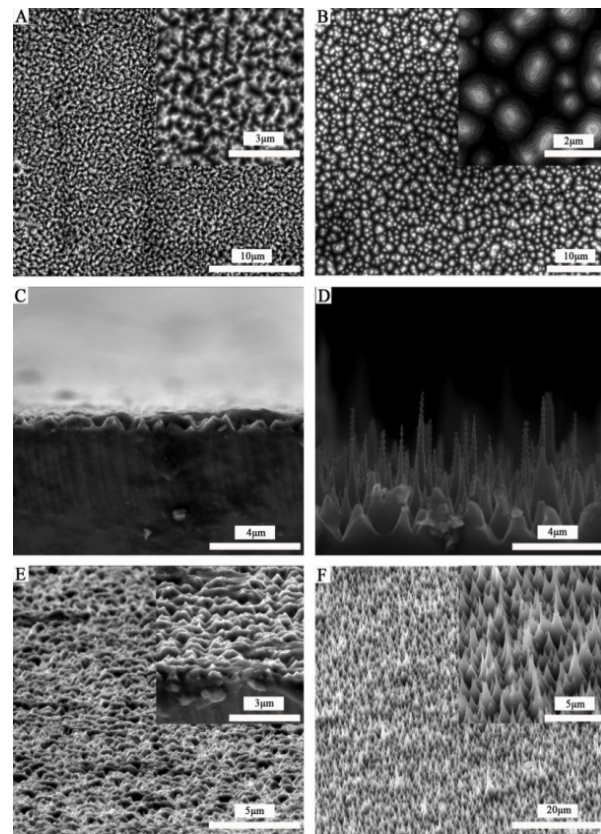


Fig. 2. Scanning electron microscopy micrographs depicting the grass. Left: (A, C and E) show top view, cross-sectional view and tilt view SEM of low aspect ratio prepared by RIE process (The etching duration is 30 min) . Right:(B, D and F) show top view, cross-sectional view and tilt view SEM of high aspect ratio prepared by DRIE process (total etch time of 8 min for the 30min RIE sample).

In the $\text{SF}_6/\text{O}_2/\text{C}_4\text{F}_8$ plasma of DRIE process, the real profile of the sidewall is not vertical, is scalloped, and the bottom of the trench is bowl-shaped due to the cyclic nature of the Bosch process[29]. Fig. 3A shows the measured reflectance spectra of the silicon grass etched using the RIE with different durations and DRIE process. The specular reflectance was evaluated on a spectrometer attached to standard mirror reflection optics at an incidence angle of 8° . For comparison, the reflectance spectrum of the Si substrate is also shown. The flat silicon wafer exhibited more than 35% reflectance in the range 300–1500 nm due to the high refractive index in the visible and infrared region (the magenta right triangle in Fig. 3(A)). The reflectance at wavelengths below 400 nm was abruptly changed because the Si has a quite high refractive index around $\lambda = 370$ nm. For RIE etched structures, the reflectance was considerably reduced over a wide wavelength range of 300–1500 nm compared to the bare Si. The silicon grass etched 10min by RIE exhibited relatively high reflectance values of $>25\%$ at wavelengths of 300-1500 nm (the black solid square in Fig. 3(A)). After Silicon etching 20 min using RIE, the grass on silicon substrate indicated the reflectance spectrum more than 10% at wavelength of 300-1500nm.

For the sample with 30 min RIE, low reflectivity of 10 % is also obtained in part of the measured wave band. Currently, we found from the measurement that the antireflection properties cannot be improved by further prolonging the RIE run beyond 30 min.

Because it is well-known that achieving a high aspect ratio tapered shape offers a better suppression of reflection. However, the aspect ratio cannot be increased by further extending the RIE etching duration, which means that the optimal etching duration is 30min in the first RIE step. The red circle in Fig. 3A shows the measured reflection from 30min RIE sample then etched by DRIE step. The sample exhibits much lower reflection ($<1\%$) over the whole spectrum, indicating broadband antireflection. In 400-1500nm wavelength range, the smallest reflectance is achieved on the grass with the high aspect ratio and the average reflectance is $<0.5\%$ (Fig. 3B). The surface of the Si substrate with fabricated grass in square pieces of Fig. 3C seems black due to the low reflectance while the bare silicon wafer reflects the image of the finger that took this picture due to the high reflectance. The square pieces silicon substrate was completely filled with random grass, similar to those in Fig. 3D.

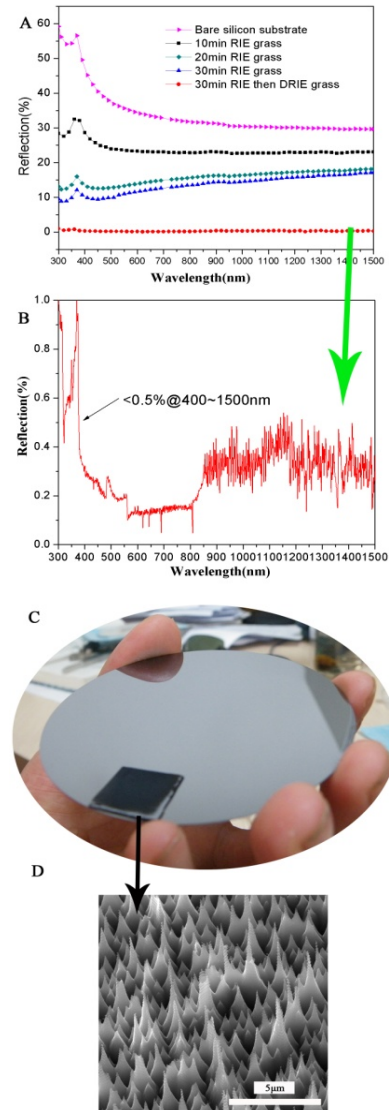


Fig. 3. (A) measured reflectance spectra of Si random grass etched by RIE at different duration and DRIE. (B) measured reflectance spectra of Si random grass etched by 30 min RIE and then 8min DRIE. Note the green arrow. (C) Si substrate with fabricated grass (square piece) is compared to bare Si substrate (wafer). Due to the low reflectance of the grass structure, sample (square piece) seems completely black, while the highly reflective bare Si substrate (wafer) reflects the image of the figure that took this picture. (D) SEM image of the grass on the square piece, note the black arrow.

The silicon grass arrays with high aspect ratio could also significantly enhance the hydrophobicity of the substrate surface due to the high fraction of air trapped in the trough area between grasses. Figure 4 exhibits the water wetting behavior of the silicon grass surfaces. Figure 4 A, B and C show water drop profiles on silicon grass surfaces within 0s, 1min and 2min, respectively. And the measured apparent water contact angle reached close to ca. 180° . Fig. 4D shows the sliding (indicated by purple arrow tip) and stationary (indicated by yellow arrow tip) water drop profile on silicon grass surface respectively. The area below the line indicated by the white line, which is the borderline between the nanostructured and the unstructured part of the Si wafer surface, possess good water-repellent properties, and the water drop can easily slide with no residual water when it has an initial velocity on the surface.

We can use the Cassie-Baxter equation[30]: $\cos\theta_c = f_s \cos\theta_s + f_a$, to interpret the evolution of contact angles, in which θ_s is the contact angle on planar silicon substrate, θ_c is the contact angle on the silicon grass surfaces, f_s and f_a are the fractions of silicon and air in contact with liquid, respectively (i.e., $f_s + f_a = 1$). The f_a fraction of air trapped in the trough area between arrays was close to 1(Figure2 D), therefore the contact angle of the sample approached 180° .

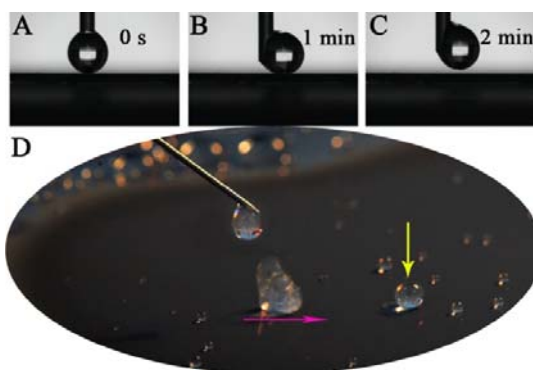


Fig. 4 (A, B and C) Still images from video contact angle measurements for a water droplet ($3\mu\text{L}$) can not adhere on the grass surfaces, (D) Optical image of water droplets of different sizes and a sliding water droplet (indicated by purple arrow tip) on the grass structure surface, exhibiting superhydrophobicity.

4. Conclusion

We have demonstrated a two-step dry etching method to synthesize random cone-shaped grass structures on silicon surface. In the first step, the low aspect ratio grass structure was prepared by RIE process, and then the grass structure was extended to high aspect ratio grass by DRIE process. The high aspect ratio grass structures show a low reflectance of about 0.5% over a

broad wavelength range of 300–1500 nm. At the same time, the silicon grass surface shows high-quality superhydrophobicity properties. And the contact angle of the grass surface approached 180° . The fabrication process of these grasses uses standard silicon fabrication methods and is conducive for integration with batch-fabricated silicon devices.

Acknowledgment

This work was supported by funds from State Key Laboratory of Ultra-Precision Machining Technology foundation of CAEP (ZZ13021), National Natural Science Foundation of China (No. 60908023), Science and Technology Development Foundation of Chinese Academy of Engineering Physics (No. 2010B0401055).

Reference

- [1] S. Chattopadhyay, Y. F. Huang, Y. J. Jen, A. Ganguly, K. H. Chen, L. C. Chen, *Materials Science & Engineering R-Reports* **69**, 1 (2010).
- [2] S. Y. Kuo, M. Y. Hsieh, H. V. Han, F. I. Lai, T. Y. Chuang, P. C. Yu, C. C. Lin, H. C. Kuo, *Opt. Express* **22**, 2860 (2014).
- [3] H. A. Macleod, *Thin-film optical filters*. Third edition (2001).
- [4] L. Yao, J. H. He, *Prog. Mater. Sci.* **61**, 94 (2014).
- [5] S. Chaudhuri, D. Bhattacharyya, A. B. Maity, A. K. Pal, *Surface coatings for solar application, Surface Coatings for Advanced Materials*, R. P. Agarwala, ed. p. 181, 1997.
- [6] H. Kikuta, H. Toyota, W. Yu, *Optical Review* **10**, 63 (2003).
- [7] X. Ye, J. Huang, J. C. Zhang, X. D. Jiang, W. D. Wu, W. G. Zheng, *J. Optoelectron. Adv. Mater.* **13**, 532 (2011).
- [8] R. Brunner, O. Sandfuchs, C. Pacholski, C. Morhard, J. Spatz, *Laser Photon. Rev.* **6**, 641 (2012).
- [9] W. J. Yang, H. C. Yu, Y. G. Wang, *J. Opt.* **15**, 055707 (2013).
- [10] L. G. Xu, Z. Geng, J. H. He, G. Zhou, *ACS Appl. Mater. Interfaces* **6**, 9029 (2014).
- [11] K. H. Nielsen, D. K. Orzol, S. Koynov, S. Carney, E. Hultstein, L. Wondraczek, *Sol. Energy Mater. Sol. Cells* **128**, 283 (2014).
- [12] L. Martinu, D. Poitras, *J. Vac. Sci. Technol. A* **18**, 2619 (2000).
- [13] Y. F. Li, J. H. Zhang, B. Yang, *Nano Today* **5**, 117 (2010).
- [14] E. B. Grann, M. G. Moharam, D. A. Pommet, *Journal of the Optical Society of America a-Optics Image Science and Vision* **11**, 2695 (1994).

- [15] Y. M. Song, H. J. Choi, J. S. Yu, Y. T. Lee, *Opt. Express* **18**, 13063 (2010).
- [16] J. Q. Xi, M. F. Schubert, J. K. Kim, E. F. Schubert, M. F. Chen, S. Y. Lin, W. Liu, J. A. Smart, *Nat. Photonics* **1**, 176 (2007).
- [17] J. Amako, D. Sawaki, E. Fujii, *Laser-Based Micro- and Nanopackaging and Assembly V*, W. Pflöging, Y. Lu, K. Washio, J. Amako, W. Hoving, eds. Spie-Int Soc Optical Engineering, Bellingham, 2011.
- [18] T. Mori, K. Hasegawa, T. Hatano, H. Kasa, K. Kintaka, J. Nishii, *Opt. Lett.* **33**, 428 (2008).
- [19] Y. Kanamori, M. Sasaki, K. Hane, *Opt. Lett.* **24**, 1422 (1999).
- [20] X. Zhang, J. Zhang, Z. Ren, X. Li, X. Zhang, D. Zhu, T. Wang, T. Tian, B. Yang, *Langmuir* **25**, 7375 (2009).
- [21] H. Sai, H. Fujii, K. Arafune, Y. Ohshita, M. Yamaguchi, Y. Kanamori, H. Yugami, *Appl. Phys. Lett.* **88**, (2006).
- [22] J. W. Leem, J. S. Yu, *Thin Solid Films* **519**, 3792 (2011).
- [23] S. Wang, X. Z. Yu, and H. T. Fan, *Appl. Phys. Lett.* **91**, 061105 (2007).
- [24] W. L. Min, B. Jiang, P. Jiang, *Advanced Materials* **20**, 3914 (2008).
- [25] H. H. Lin, W. H. Chen, F. C. N. Hong, *Journal of Vacuum Science & Technology B* **31**, 031401 (2013).
- [26] E. B. Grann, M. G. Moharam, *Journal of the Optical Society of America a-Optics Image Science and Vision* **13**, 988 (1996).
- [27] R. Pinto, K. V. Ramanathan, R. S. Babu, *J. Electrochem. Soc.* **134**, 165 (1987).
- [28] H. Jansen, M. Deboer, R. Legtenberg, and M. Elwenspoek, *Journal of Micromechanics and Microengineering* **5**, 115 (1995).
- [29] C. L. Chang, Y. F. Wang, Y. Kanamori, J. J. Shih, Y. Kawai, C. K. Lee, K. C. Wu, M. Esashi, *Journal of Micromechanics and Microengineering* **15**, 580 (2005).
- [30] X. J. Feng, L. Jiang, *Advanced Materials* **18**, 3063 (2006).

*Corresponding author: yehanwin@mail.ustc.edu.cn